CMOS-MEMS prestress vertical cantilever resonator with electrostatic driving and piezoresistive sensing

Jin-Chern Chiou, Li-Jung Shieh and Yung-Jiun Lin

Department of Electrical and Control Engineering, National Chiao Tung University, Hsin-Chu, Taiwan, Republic of China

E-mail: chiou@mail.nctu.edu.tw, ljs.ece93g@nctu.edu.tw and yjlin@mail.nctu.edu.tw

Abstract

This paper presents a CMOS-MEMS prestress vertical comb-drive resonator with a piezoresistive sensor to detect its static and dynamic response. The proposed resonator consists of a set of comb fingers fabricated along with a composite beam. One end of the composite beam is clamped to the anchor, while the other is elevated by residual stress. Actuation occurs when the electrostatic force, induced by the fringe effect, pulls the composite beam downwards to the substrate. The initial tip height at the free end of the resonator due to residual stress is approximately 60 μm. A piezoresistor is designed to sense the vertical deflection and vibration of the resonator. The relative change in the resistance of the piezoresistor ($\Delta R/R$) is about 0.52% when a voltage of 100 V is applied in static mode. The first resonant frequency of the device is 14.5 kHz, and the quality factor is around 36 in air. The device is fabricated through TSMC 0.35 μm 2p4m CMOS process and post-CMOS process.

(Some figures in this article are in colour only in the electronic version)

1. Introduction

Micromachined resonators have been widely investigated and are currently employed in various applications such as temperature, humidity and gas detection, as well as in biological technology and other applications [1–4]. In most resonators, not only resonance frequency but also vibration amplitude, phase and quality factor are detected. However, frequency is the most commonly used resonator signal output since its quasi-digital form supports unproblematic signal transfer and precise readout [5].

Among the existing excitation methods for MEMS resonators that were previously proposed are included thermal, piezoelectric, electromagnetic and electrostatic [5, 6]. Thermal excitation is based on the difference between the thermal expansions of different materials in a composite cantilever beam. This excitation principle is easy to implement, but requires high power consumption [7]. Piezoelectricity is the most often utilized phenomenon to excite a resonator. However, piezoelectric materials may cause

hysteresis and are not compatible with the CMOS process [8, 9]. Electromagnetic actuation consumes less power than thermal excitation, if the external magnetic field is sufficiently strong. Nevertheless, it complicates the production process because a permanent magnet needs to be integrated into the device [6, 10]. Electrostatic excitation is also widely used in micromachined devices [11–14]. The main benefit of electrostatic excitation is its characteristic of low power consumption. Recently, many electrostatic actuation methods have been developed, such as the parallel plate, lateral comb-drive and vertical comb-drive structures. A vertical resonator with a parallel plate electrostatic actuator exhibits a nonlinear phenomenon, called pull-in, which severely constrains the stable region at one-third the length of the gap [15]. Electrostatic comb actuators were developed to avoid pull-in. The comb-drive structure has an advantage over parallel plates, in that the electrostatic force is independent of the displacement of the actuator. Therefore, the positioning of the comb-drive shuttle can be controlled accurately using the applied voltage.
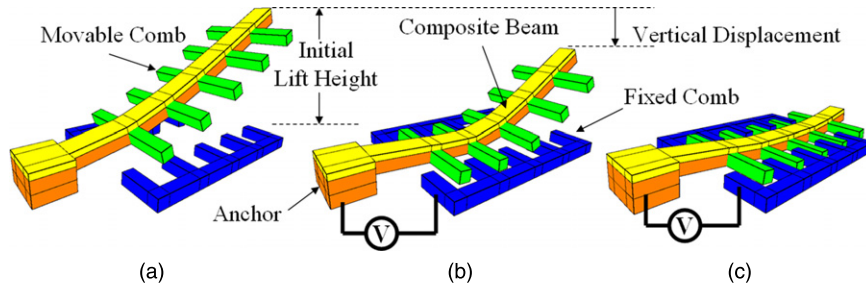
J. Phys. D: Appl. Phys. **41** (2008) 205102

J-C Chiou *et al*

Figure 1. The resonator at different driving states: (*a*) initial state, (*b*) bias voltage state, (*c*) critical bias voltage state.

Besides excitation methods, sensing methods are also an important issue in designing a resonator. Several techniques have been proposed for measuring the bending or vibration of a cantilever resonator. They include optical and piezoresistive detection [16]. The most frequently used method is optical detection [17–19] because of its inherent simplicity and high sensitivity. However, its disadvantages include problems with alignment capability, miniaturization and portability. Another useful technique is piezoresistive detection [20–22]. The resistance of the piezoresistor varies with the surface stress-induced deflection of cantilever. The measurement can be integrated by using the piezoresistor for the sensing element.

With regard to CMOS-MEMS technology, it has been developed over the past decade. Monolithic integration of microdevices with electronics can not only lower manufacturing cost but also minimize total systems. The parasitic resistance and capacitance associated with the interconnection between the MEMS devices and electronics can also be reduced. It is conductive to enhance electrical signal quality and improve system performance. A famous example is the digital micromirror device (DMD) made by Texas Instruments [23].

This investigation develops a vertical resonator with electrostatic driving and piezoresistive sensing. CMOS-MEMS technology is used for fabrication. In the following sections, the operating principle, modelling and simulation and fabrication are given. Experimental results indicated that the present resonator possesses a 14.5 kHz resonating frequency and a quality factor of around 36 in air.

2. Operating principle

2.1. Electrostatic actuation

The electrostatic actuation method of the developed resonator is based on a prestress comb-drive structure [24]. Figure 1 schematically depicts a resonator with different driven states. The resonator consists of an anchor, a composite beam and a set of comb fingers. These comb fingers, designed along the composite beam, act as the movable and fixed comb fingers. Figure 1(*a*) shows one end of the composite beam, which is clamped to the anchor, and the other end is elevated due to the residual stress between the two deposited materials. Notably, the initial lift height of the resonator can be further enhanced by increasing the residual stress of the composite

beam using a post heat treatment process [25]. When a voltage, *V*, is applied between the movable and fixed comb, the movable composite beam can be pulled downwards to the substrate by the electrostatic force induced by the fringe effect, as shown in figure 1(*b*). The taper-like distances between each movable and fixed comb are obtained from the free end to the fixed end based on the curved-up shape of the composite beam. In the actuating mechanisms, the movable comb fingers that are close to the anchor provide the main actuation force. As the actuation progresses, these movable comb fingers will be pulled down accordingly. As the driving voltage is increased, the vertical displacement of the free end of the resonator is increased. Compared with the parallel plate electrostatic actuator, the vertical comb drive exhibits no pull-in and hysteresis phenomenon. Notably, the electrostatic force is constrained when the movable comb finger is close to the fixed comb finger, independently of the input driving voltage, as shown in figure 1(*c*).

2.2. Piezoresistive detection

Piezoresistivity is a material property that is exhibited when a mechanical stress applied to the material affects the bulk resistivity [26]. The change in resistivity due to mechanical stress is called the piezoresistive effect. Silicon, especially in the monocrystalline form, exhibits a strong piezoresistive characteristic. It also has excellent mechanical properties, which makes it a suitable material for a piezoresistive sensing element. For instance, a strain gauge is a typical example of the application of the piezoresistive effect [27].

For a piezoresistor, the resistance is associated with stress that is longitudinal (σ_l) and transverse (σ_t) with respect to the current flow. Assuming that the mechanical stresses are constants over the piezoresistor and the geometric changes are neglected, the relative change in the resistance *R* is given by [26]

$$\frac{\Delta R}{R} = \sigma_l \pi_l + \sigma_t \pi_t, \tag{1}$$

where π_l and π_t are the longitudinal and transverse piezoresistive coefficients, respectively. The two coefficients depend on the crystal orientation, the doping type and the concentration. The output signal from the piezoresistor is usually measured using a Wheatstone bridge and the variation of the piezoresistor (ΔR) can be transformed to a voltage output. Figure 2 depicts the Wheatstone bridge configuration

of four resistors. The output voltage V_{out} of the Wheatstone bridge is given by

$$V_{out} = \frac{1}{4}\frac{\Delta R}{R}V_{in}, \qquad (2)$$

where V_{in} is the supply voltage, R is the initial resistance of the piezoresistor and ΔR is the change in resistance. Equation (2) has shown an important advantage of the Wheatstone bridge configuration: the output voltage is independent of the absolute value of the piezoresistor. It is determined merely by the relative change in resistance and the supply voltage.

3. Modelling and simulation

3.1. Theoretical analysis and modelling

The cantilever composite beam consists of two materials A and B that possess tensile and compressive residual stress, respectively, as shown in figure 3(*a*). With the released processes, the composite beam is assumed curving up with the lift height, H_L, at the free end due to the induced stresses. In the present derivations, the symbols a_n, P_n, H_{Fn}, L are denoted as the distance related to the anchor, electrostatic force induced by the comb finger 1–n in kth and $(k-1)$th state, lift height of the nth movable comb finger and length of the composite beam, respectively. Here, one-movable and two-fixed comb fingers were defined as a single pair of comb fingers for the purpose of simulating and extracting capacitance function during electrostatic force calculation. A cross section view of the composite beam is shown in figure 3(*b*), where L_C is the engaged length between the movable and fixed comb fingers.
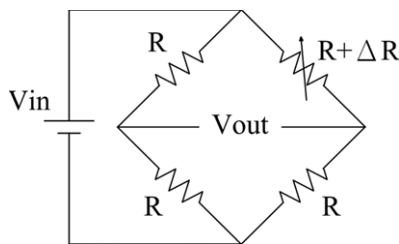

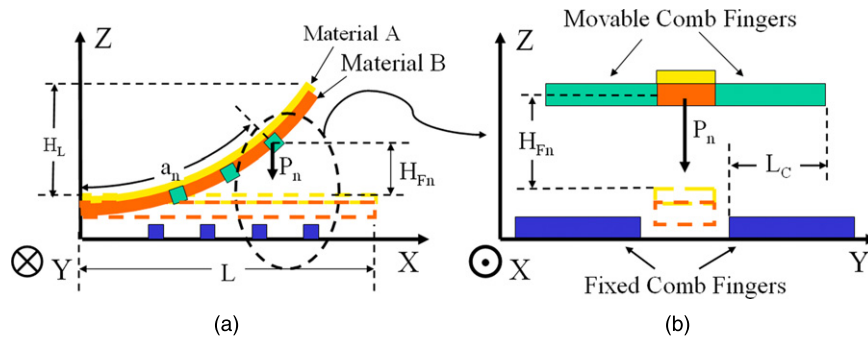**Figure 2.** The Wheatstone bridge configuration of four resistors.

3.1.1. Decomposition of multiple loads. In the mechanics of material analysis, the deflection of a straight beam with constant multiple loads can be calculated as follows [28]:

$$\begin{cases} z_{xn} = \dfrac{P_n \cdot x^2}{6 \cdot E_c \cdot I_c}(3 \cdot a_n - x), \\[2mm] z'_{xn} = \dfrac{P_n \cdot x}{2 \cdot E_c \cdot I_c}(2 \cdot a_n - x), \end{cases} \quad \text{for } 0 \leqslant x \leqslant a_n, \quad (3)$$

$$\begin{cases} z_{xn} = \dfrac{P_n \cdot a_n^2}{6 \cdot E_c \cdot I_c}(3 \cdot x - a_n), \\[2mm] z'_{xn} = \dfrac{P_n \cdot a_n^2}{2 \cdot E_c \cdot I_c}, \end{cases} \quad \text{for } a_n \leqslant x \leqslant L, \quad (4)$$

where x is the position of the beam, Z_{xn} is the shape of small deflection of the strength beam at position x coming from the nth load, Z'_{xn} is the slope of shape at position x coming from the nth load, a_n is the position of the nth load, P_n is the difference in the electrostatic force induced by the comb finger 1–n in the kth and the $(k-1)$th state, E_C is Young's modulus of an equivalent single material beam and I_C is the moment of inertia of an equivalent single material beam. The following section discusses the equivalent material parameters and electrostatic force.

3.1.2. Moment of inertia of composite beam. In order to accurately calculate the moment of inertia of the designed beam, the composite beam can be recast into a T shape single beam as shown in figure 4. The material A with width b was replaced by material B with width $\alpha \cdot b$, where b is the width of the composite beam, α is the proportional constant between Young's modulus of materials A and B, h_1 is the distance between the top side of material A and the neutral axis of the T shape beam and h_2 is the distance between the bottom side of material B and the neutral axis of the T shape beam. The moment of inertia of the T shape beam can be expressed as [28]

$$I_c = \frac{1}{12} \cdot b \cdot t_A^3 + b \cdot t_A \cdot \left(h_1 - \frac{t_A}{2}\right)^2$$

$$+ \frac{1}{12} \cdot (\alpha \cdot b) \cdot t_B^3 + \alpha \cdot b \cdot t_B \cdot \left(h_2 - \frac{t_B}{2}\right)^2, \quad (5)$$

where $E_C = E_B$, $\alpha = E_B/E_A$, $h_1 = (t_A \cdot A_A + t_B \cdot A_B)/(A_A + A_B)$, $h_2 = t_A + t_B - h_1$ and A_A and A_B are the cross-section areas of materials A and B, respectively.

Figure 3. A schematic view of the composite beam: (*a*) the *XZ* plane cross-section view, (*b*) the *YZ* plane cross-section view (a single pair of comb finger).
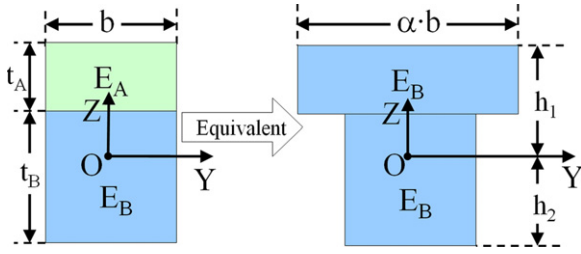
Figure 4. The equivalent beam model of the composite beam.

3.1.3. Resonant frequency of composite beam. The resonant frequency of a homogeneous cantilever beam with uniform cross-section is defined as [29]

$$f_n = \frac{\lambda_n^2}{2\pi L^2} \sqrt{\frac{EI}{\rho A}}, \tag{6}$$

where λ_n is a dimensionless parameter, which is determined by the boundary conditions, and L, E, I, ρ and A are the length, Young's modulus, moment of inertia about the neutral axis, density and area of cross-section of the cantilever beam, respectively. Composite beams may be analysed using the same theory as is used for ordinary beams, since the assumption that plane cross-sections remain plane after bending is valid in pure bending, independently of the material [28]. Therefore, the natural frequency of a composite beam can be approximated by

$$f_n = \frac{\lambda_n^2}{2\pi L^2} \sqrt{\frac{\sum_{i=1}^{N} E_i I_i}{\bar{\rho} A}}, \tag{7}$$

where N is the number of layers in the composite beam, E_i and I_i are the Young's modulus and the moment of inertia of each layer and $\bar{\rho}$ is the average specific mass density of the composite beam, which is given by

$$\bar{\rho} = \frac{\sum_{i=1}^{N} \rho_i t_i}{\sum_{i=1}^{N} t_i}, \tag{8}$$

where ρ_i and t_i are the density and thickness of each layer, respectively. The theoretical resonant frequency of the resonator is calculated at 15.7 kHz by using equation (7).

3.2. FEM mode simulation

To fully understand the resonant characteristics of the resonator, an FEM simulator, IntelliSuite®, is used to calculate the resonant frequencies and the corresponding mode shapes. The resonator consists of a $500 \times 44\,\mu\mathrm{m}^2$ composite beam that is fixed to an anchor structure with 34 movable comb fingers orthogonally mounted on the composite beam, and 35 fixed comb fingers are mounted on the silicon substrate. The dimension of the comb finger is $68 \times 3.6\,\mu\mathrm{m}^2$, and the overlap length is $60\,\mu\mathrm{m}$. Note that in the present FEM simulations, we solely require a movable comb and composite beam to calculate the resonant frequencies. Table 1 shows the mode shape simulation results of the proposed resonator. In the first mode, the resonator is bending in the vertical direction.

The second mode is yaw and roll motion; attention must be paid to avoid shorting due to the contact between movable and fixed combs. In the third mode, the resonator is vibrating in roll motion. These simulation results can be used as the reference data in determining the resonant modes during the actual experimental measurements.
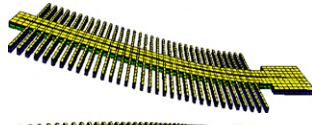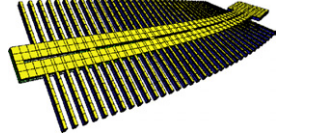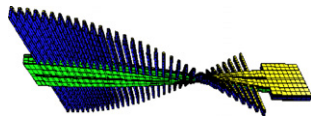
4. Fabrication

The proposed resonator device was fabricated through TSMC (Taiwan Semiconductor Manufacturing Company) $0.35\,\mu\mathrm{m}$ 2p4m (double polysilicon quadruple metal) CMOS process and post-CMOS micromachining process, which was provided by the National Chip Implementation Center (CIC) [30]. The CMOS process consists of two polysilicon layers, four metal layers, three via layers and several dielectric layers. All metal layers are made of aluminium and the contact/via holes are filled with tungsten plugs. The dielectric layers are silicon dioxide and the passivation layer includes silicon dioxide and silicon nitride. The etched holes are filled with silicon dioxide. The field oxide (FOX) layer is silicon dioxide. In order to fabricate a flat plane surface, chemical mechanical polishing (CMP) is employed after each deposition layer was completed.

After the CMOS process, a post-CMOS micromachining process which includes a 2-step dry etching is used to release the suspended structures of MEMS devices. Figure 5(*a*) illustrates the cross-section view of the MEMS components fabricated through the TSMC $0.35\,\mu\mathrm{m}$ 2p4m CMOS process. Before the dry etching steps, a thick PR layer is coated on the chip and patterned as illustrated in figure 5(*b*). This PR mask is utilized to protect the bonding pads, electronic circuit and the not needed etched regions of the MEMS components during dry etching processes. After the PR mask is completed, an anisotropic reactive-ion etch (RIE) with CHF_3/O_2 plasma is used to define the sidewalls of the device structure and etch the silicon dioxide in the etching holes, respectively. Figure 5(*c*) schematically shows the cross-section view of the MEMS device after the anisotropic RIE process. Then an isotropic RIE with SF_6/O_2 is applied to etch the silicon substrate and release the suspended structures of the MEMS components. Finally, the PR mask is removed to complete the post-CMOS micromachining process, as shown in figure 5(*d*).

In order to enhance the electrostatic force, the thickness of the comb fingers must be increased. Therefore, the designed comb fingers consist of all conductive layers in the CMOS process. Figure 6 illustrates the cross-section of the comb fingers. Besides, the composite beam is made of M3, M4 and all dielectric layers. Since it is made of multiple material layers, it is bent due to residual stress. The piezoresistor made of polysilicon (Poly2) is at the fixed end of the composite beam and the resistance is about $52\,\mathrm{k}\Omega$. For this design, we consulted the sheet resistance of the two polysilicon layers as given in the TSMC $0.35\,\mu\mathrm{m}$ 2p4m CMOS process datasheet. The sheet resistance of Poly1 is $8\,\Omega/\mathrm{sq}$ and Poly2 is $50\,\Omega/\mathrm{sq}$. Therefore, Poly2 is more suitable as a piezoresistor than Poly1. Figure 7 displays the fabricated resonator device produced by the CMOS process and the post-CMOS micromachining. It is bent by the residual stress, as predicted, and the initial tip height at the free end is around $60\,\mu\mathrm{m}$.

Table 1. The mode shape of the resonator.

Mode	Frequency (Hz)	Motion	Solid mode shape
First	16790.7	Pitch	
Second	103433	Yaw and roll	
Third	105726	Roll	

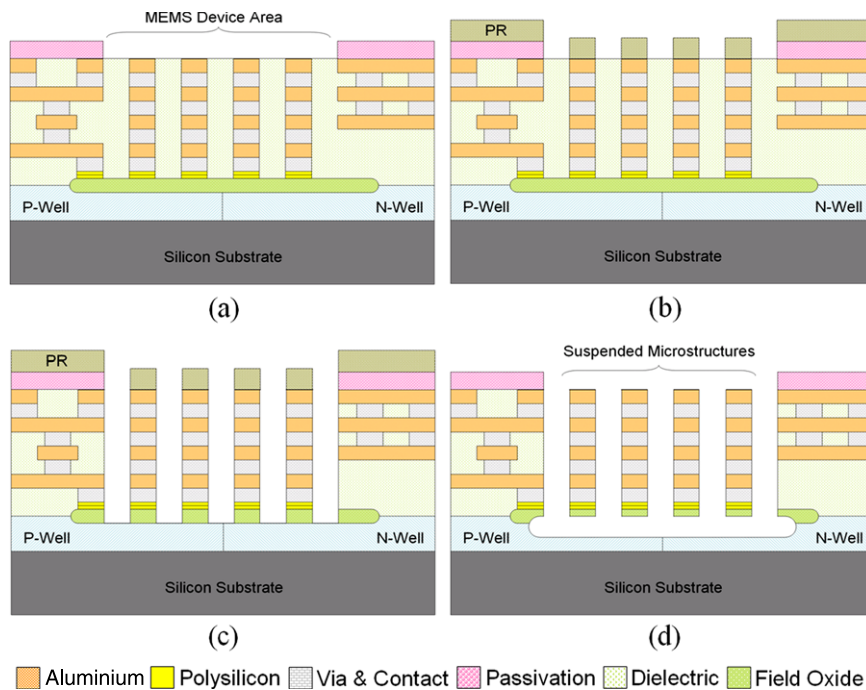Aluminium   Polysilicon   Via & Contact   Passivation   Dielectric   Field Oxide

Figure 5. Process flow: (*a*) completion of CMOS process, (*b*) patterning a PR mask to protect unneeded etched regions, (*c*) etching silicon dioxide by anisotropic RIE etching, (*d*) etching silicon substrate to release suspended microstructure and remove the PR (colour online).

5. Experiment and discussion

5.1. Static characteristic measurement

In order to examine the static characteristics of the resonator device, a WYKO interferometer and an LCR meter are used for preliminary measurement. The experimental block diagram is shown in figure 8. To actuate the resonator using the electrostatic force, a dc bias driving voltage given by the power amplifier is used. As expected, the variation of resistance due to the piezoresistive effect occurred with the deflection of the resonator. The WYKO interferometer and LCR meter are utilized to measure the vertical displacement and the piezoresistor variation of the resonator, respectively. The tip height at the free end of the resonator versus the applied dc bias driving voltage between movable and fixed combs is shown in figure 9. The vertical displacement decreased from 61.9

to 58.4 μm and was obtained when driving the device with a voltage ranging from 0 to 100 V; thus, a maximum vertical displacement of 3.5 μm is observed. The variation of the piezoresistor is also shown in figure 9. The resistance value increased from 52.19 to 52.46 kΩ and was obtained when driving the device with a voltage ranging from 0 to 100 V. The maximum relative resistance change of the piezoresistor ($\Delta R/R$) is about 0.52% when the applied voltage is 100 V, as shown in figure 10. The result indicates that the piezoresistor possesses a linear characteristic between 40 and 100 V.

5.2. Frequency response measurement

Figure 11 shows the frequency response of the resonator that is measured by using an MEMS Motion Analyzer (MMA) and a piezoresistor, respectively. The piezoresistor output is connected to an external Wheatstone bridge (5 V supply
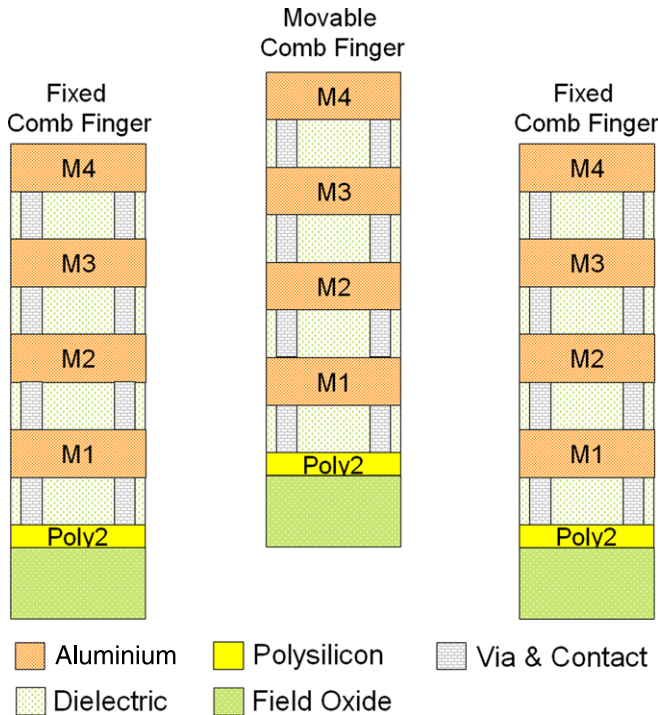
J. Phys. D: Appl. Phys. **41** (2008) 205102

J-C Chiou *et al*

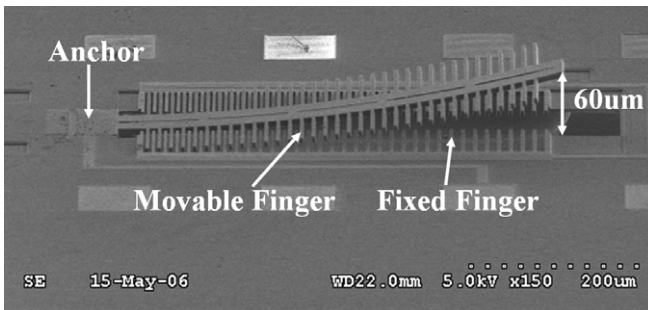**Figure 6.** Cross-section of the fixed and movable comb fingers (colour online).

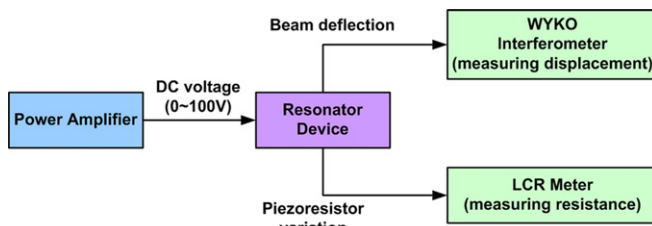**Figure 7.** SEM image of a fabricated resonator device.

Figure 8. The experimental diagram of static characteristic measurement.

voltage) and a commercial instrumentation amplifier (AD620) with a gain of 25. The resonator is biased by a sinusoidal wave with voltage offset of 30 V and amplitude of 30 V, and the frequency ranges between 5 and 20 kHz. The first resonant frequency mode is measured at 14.5 kHz, and it closely matches the calculation (15.7 kHz) and simulation result (16.8 kHz). The error is due to fabrication process variations such as the thickness of each layer and the undercut of silicon. The beam length is increased due to the undercut
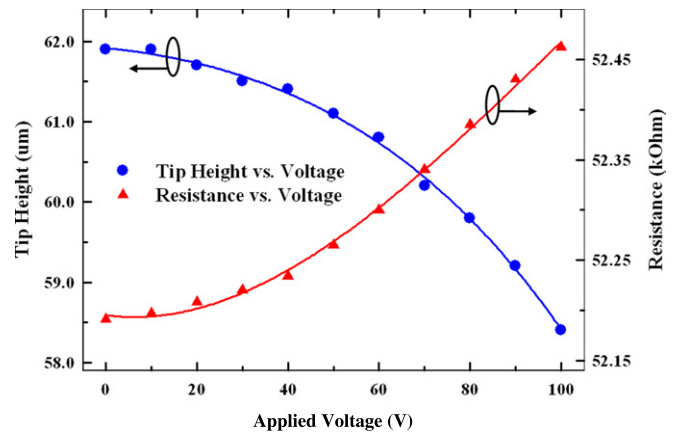

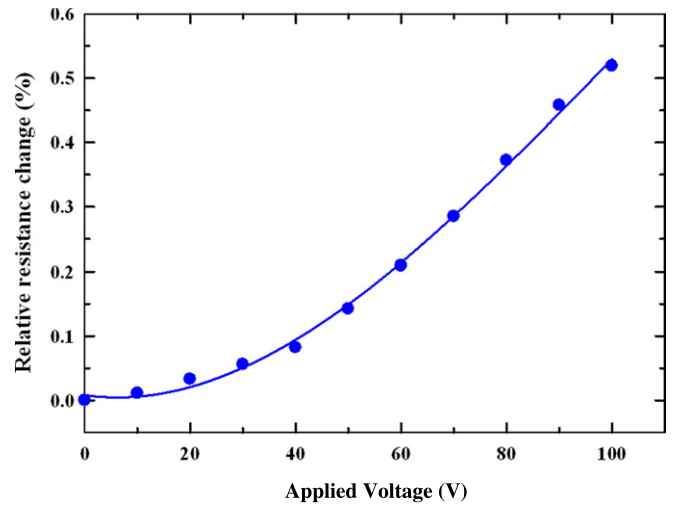**Figure 9.** The static characteristic of the resonator.

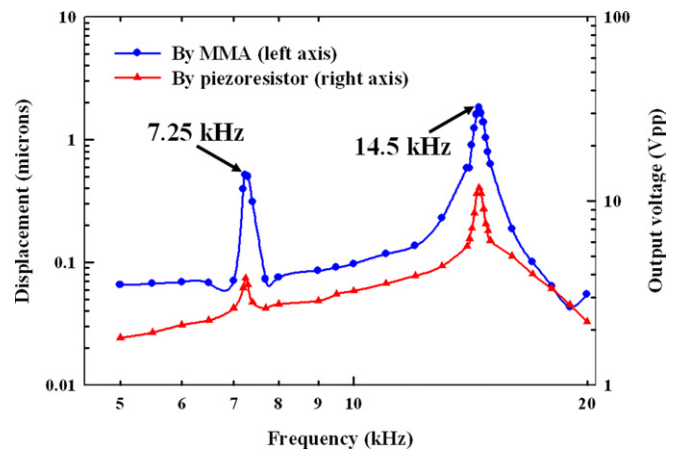**Figure 10.** The relative resistance change ($\Delta R/R$) of the piezoresistor.

Figure 11. The frequency response of the resonator.

phenomenon which results in the decrease in the spring constant. Thus the measured resonant frequency is lower than the simulated result. The quality factor is calculated at 36. The results indicate that the piezoresistor and MMA measurements coincide on the resonance. The piezoresistive signal completely reflects the mechanical vibrations of the

resonator. Besides, the power consumption of the Wheatstone bridge is about 0.48 mW. Notably, a 'half mode' peak before the first mode peak resonance in 7.25 kHz is also observed in this measurement. The half mode characteristic is due to the double frequency and nonlinear effect in the electrostatic resonator [31, 32]. It occurs when a driving voltage of the ac signal coupled with dc bias is used to eliminate the frequency distortion which caused when the resonator is driven by a pure ac signal. It exists not only in electrostatic actuation but also in other actuation principle such as electromagnetic, thermo and piezoelectric actuators [33, 34]. However, devices generally do not work at half mode. Thus, it is unnecessary to suppress the half mode.

6. Conclusions

This work presents a vertical comb-drive resonator with a piezoresistor sensing component. The static characteristic and frequency response of the resonator are measured. The proposed resonator device is implemented using the TSMC 0.35 μm 2p4m CMOS process and the post-CMOS process. The design, modelling, simulation and measurement are also presented. Preliminary measurement demonstrates that the initial lift height by residual stress is about 60 μm and the resonant frequency is 14.5 kHz. The measurement results also indicate that the piezoresistor produced by Poly2 possesses a good piezoresistive characteristic. In the future, the resonator could be used as a sensor or an actuator.

Acknowledgments

References

[1] Fritz J, Baller M K, Lang H P, Rothuizen H, Vettiger P, Meyer E, Guntherodt H J, Gerber C and Gimzewski J K 2000 Translating biomolecular recognition into nanomechanics *Science* **288** 316–8

[2] Zhang H and Kim E S 2005 Micromachined acoustic resonant mass sensor *J. Microelectromech. Syst.* **14** 699–706

[3] Bedair S S and Fedder G K 2004 CMOS MEMS oscillator for gas chemical detection *Proc. IEEE Sensors (Vienna, Austria)* pp 955–8

[4] Godin M, Bryan A K, Burg T P, Babcock K and Manalis S R 2007 Measuring the mass, density, and size of particles and cells using a suspended microchannel resonator *Appl. Phys. Lett.* **91** 123121

[5] Buser R A 1994 Resonant sensors *Mechanical Sensors* (*Sensors: A Comprehensive Survey* vol 7) ed H H Bau *et al* (Weinheim: VCH) pp 205–84

[6] Lange D, Brand O and Baltes H 2002 *CMOS Cantilever Sensor Systems: Atomic Force Microscopy and Gas Sensing Applications* (Berlin: Springer) pp 7 and 21–2

[7] Brand O and Baltes H 1993 Thermally excited silicon oxide beam and bridge resonators in CMOS technology *IEEE Trans. Electron Devices* **40** 1745–53

[8] Yan L, Pang W, Wu J, Tang W C and Kim E S 2004 High frequency micromechanical piezo actuated disk resonator *Proc. Solid-State Sensor, Actuator and Microsystems Workshop (Hilton Head Island, SC)* pp 372–5

[9] Kawai Y, Ono T, Esashi M, Meyer E and Gerber C 2007 Resonator combined with a piezoelectric actuator for chemical analysis by force microscopy *Rev. Sci. Instrum.* **78** 063709

[10] Vancura C, Ruegg M, Li Y, Lange D, Hagleitner C, Brand O, Hierlemann A and Baltes H 2003 Magnetically actuated CMOS resonant cantilever gas sensor for volatile organic compounds *Proc. 12th Int. Conf. on Solid State Sensors, Actuators and Microsystems (Boston, MA)* pp 1355–8

[11] Xie H, Pan Y and Fedder G K 2003 A CMOS-MEMS mirror with curled-hinge comb drives *J. Microelectromech. Syst.* **12** 450–7

[12] Li Y C, Ho M H, Hung S J, Chen M H and Lu M S C 2006 CMOS micromachined capacitive cantilevers for mass sensing *J. Micromech. Microeng.* **16** 2659–65

[13] Dai C L and Yu W C 2006 A micromachined tunable resonator fabricated by the CMOS post-process of etching silicon dioxide *Microsyst. Technol.* **12** 766–72

[14] Cheng K M, Weng Z, Oliver D R, Thomson D J and Bridges G E 2007 Microelectromechanical resonator characterization using noncontact parametric electrostatic excitation and probing *J. Microelectromech. Syst.* **16** 1054–60

[15] Pons-Nin J, Rodriguez A and Castaner L M 2002 Voltage and pull-in time in current drive of electrostatic actuators *J. Microelectromech. Syst.* **11** 196–205

[16] Lavrik N V, Sepaniak M J and Datskos P G 2004 Cantilever transducers as a platform for chemical and biological sensors *Rev. Sci. Instrum.* **75** 2229–53

[17] Battiston F M, Ramseyer J P, Lang H P, Baller M K, Gerber C, Gimzewski J K, Meyer E and Guntherodt H J 2001 A chemical sensor based on a microfabricated cantilever array with simultaneous resonance-frequency and bending readout *Sensors Actuators* B **77** 122–31

[18] Kim B H, Kern D P, Raible S and Weimar U 2002 Fabrication of micromechanical mass-sensitive resonators with increased mass resolution using SOI substrate *Microelectron. Eng.* **61–62** 947–53

[19] Muralidharan G, Wig A, Pinnaduwage L A, Hedden D, Thundat T and Lareau R T 2003 Adsorption–desorption characteristics of explosive vapors investigated with microcantilevers *Ultramicroscopy* **97** 433–9

[20] Thaysen J, Boisen A, Hansen O and Bouwstra S 2000 Atomic force microscopy probe with piezoresistive read-out and a highly symmetrical Wheatstone bridge arrangement *Sensors Actuators* A **83** 47–53

[21] Chivukula V, Wang M, Ji H F, Khaliq A, Fang J and Varahramyan K 2006 Simulation of SiO$_2$-based piezoresistive microcantilevers *Sensors Actuators* A **125** 526–33

[22] Jin D, Li X, Liu J, Zuo G, Wang Y, Liu M and Yu H 2006 High-mode resonant piezoresistive cantilever sensors for tens-femtogram resoluble mass sensing in air *J. Micromech. Microeng.* **16** 1017–23

[23] Hornbeck L J 1996 Digital light processing and MEMS: Reflecting the digital display needs of the networked society *Proc. SPIE* **2783** 2–13

[24] Chiou J C and Lin Y J 2005 A novel large displacement electrostatic actuator: pre-stress comb-drive actuator *J. Micromech. Microeng.* **15** 1641–8

[25] Chen R T, Nguyen H and Wu M C 1999 A low voltage micromachined optical switch by stress-induced bending *Proc. IEEE MEMS '99 (Orlando, FL)* pp 424–8

[26] Kloeck B 1994 Piezoresistive sensors *Mechanical Sensors* (*Sensors: a Comprehensive Survey* vol 7) ed H H Bau *et al* (Weinheim: VCH) pp 145–72

[27] Pallas-Areny R and Webster J G 2001 *Sensors and Signal Conditioning* 2nd edn (New York: Wiley) pp 80–8

[28] Gere J M and Timoshenko S P 1990 *Mechanics of Materials* 3rd edn (Boston: PWS) pp 772 and 301–8

[29] Blevins R D 1984 *Formulas for Natural Frequency and Mode Shape* (Malabar, Fl: Krieger) p 104

[30] Chiou J C, Lin Y J and Kuo C F 2008 Extending the traveling range with a cascade electrostatic comb-drive actuator *J. Micromech. Microeng.* **18** 015018

[31] Chiou J C and Lin Y J 2006 Modeling and verification of the double frequency effect using a MEMS device *Microsyst. Technol.* **12** 796–802

[32] Jin Z, Wang Y, Xu Y and Ding C 1995 The properties of micromechanical resonator *Proc. 4th Int. Conf. on Solid-State and Integrated Circuit Technology (Beijing, China)* pp 482–4

[33] Piyabongkarn D, Sun Y, Rajamani R, Sezen A and Nelson B J 2005 Travel range extension of a MEMS electrostatic microactuator *IEEE Trans. Control. Syst. Technol.* **13** 138–45

[34] Ries L L and Smith S W 1997 Phase aberration correction in two dimensions with an integrated deformable actuator/transducer *IEEE Trans. Ultrason. Ferrelectr.* **44** 1366–75